Ceplecha and P. Pecina, Eds. *Publ. Astron. Inst. Czech. Acad. Sci. No. 67*, vol. 2, p. 21 (1987); H. Rickman and Cl. Froeschlé, *Celestial Mech.* **43**, 243 (1988)].
11. This is a well-known result that comes from the quasi-conservation of the Tisserand parameter and the quasi-constancy of the semimajor axis in the absence of close encounters with Jupiter. Mathematically, this leads to: $\sqrt{a(1-e^2)}\cos i \approx$ const.
12. Cl. Froeschlé and H. Scholl, *Astron. Astrophys.* **111**, 346 (1982).
13. See A. Carusi and G. B. Valsecchi, Eds., *Dynamics of Comets: Their Origin and Evolution* (Reidel, Dordrecht, 1985).
14. Z. Sekanina discusses the distintegration of comets in *Icarus* **58**, 81 (1984) and the splitting of comets in *Comets*, L. Wilkening, Ed. (Univ. of Arizona Press, Tucson, 1982), pp. 251–287. See also the papers by L. Kresák (and references therein): in (*13*), p. 279; *Int. Comet Q.* **9**, 59 (1987).
15. B. McIntosh, paper presented at the "Comets in the Post-Halley Era" conference, Bamberg, West Germany, April 1989.
16. S. E. Hamid and M. N. Youssef, *Smithsonian Contrib. Astrophys.* **7**, 309 (1963).
17. D. W. E. Green, Ed., *Int. Comet Q.* **8**, 43 (1986); *ibid.*, p. 46; *ibid.*, p. 85; *ibid.*, p. 89; *ibid.* **9**, 80 (1987).
18. ———, T. L. Rokoske, C. S. Morris, in *Proceedings of the 20th ESLAB Symposium on the Exploration of Halley's Comet*, B. E. Battrick, E. J. Rolfe, R. Reinhard, Eds. (ESA Publication SP-250) (European Space Agency, Noordwijk, The Netherlands, 1986), vol. 3, pp. 249–251. See also D. W. E. Green and C. S. Morris, *Astron. Astrophys.* **187**, 560 (1987).
19. The detector used was an RCA 512×320 chip with 27-μm pixels. At the *f*/8.75 Cassegrain focus, this gives an image scale of 0.46″ per pixel, and a field of view of 4′ × 2.5′. The telescope was tracked to follow the motion of the comet. Most exposures were 6 or 10 min long. Absolute photometry of the images is, unfortunately, not possible, since of the four nights, only 7 July was photometric, and, on that night, only one image was taken, in which the comet overlapped a bright star trail.
20. T. X. Thuan and J. E. Gunn, *Publ. Astron. Soc. Pac.* **88**, 543 (1976).
21. G. Pizarro, O. Pizarro, R. M. West, *Minor Planet Circ. 14669* (1989). K. J. Meech, *Minor Planet Circ. 14670* (1989); magnitudes of comparison stars from A. U. Landolt, *Astron. J.* **78**, 959 (1973).
22. This is also commented upon by Z. Sekanina, *Astron. J.*, in press.
23. S. Nakano, *Minor Planet Circ. 8694* and *8695* (1984), *12025* (1987), and *12626* (1988); 16 cases of comets that were originally given minor planet designations are listed by B. G. Marsden, in *Catalogue of Discoveries and Identifications of Minor Planets* (International Astronomical Union Minor Planet Center, Smithsonian Astrophysical Observatory, Cambridge, MA, ed. 2, 1986), p. 140.
24. Useful discussions were provided by B. G. Marsden, C. M. Bardwell, and Z. Sekanina. We thank J. Briggs and the late E. Everhart, Chamberlin Observatory, University of Denver, and J. V. Scotti and T. Gehrels, Lunar and Planetary Laboratory, University of Arizona, for looking at astrometric data in search of more photometric information. We thank R. H. McNaught, Siding Spring Observatory, for searching old plates for possible images of P/Machholz. A.C.P.'s research at Caltech was supported in part by an ARCS fellowship.

14 September 1989; accepted 29 November 1989

Interparticle Collisions Driven by Ultrasound

STEPHEN J. DOKTYCZ AND KENNETH S. SUSLICK*

Ultrasound has become an important synthetic tool in liquid-solid chemical reactions, but the origins of the observed enhancements remained unknown. The effects of high-intensity ultrasound on solid-liquid slurries were examined. Turbulent flow and shock waves produced by acoustic cavitation were found to drive metal particles together at sufficiently high velocities to induce melting upon collision. A series of transition-metal powders were used to probe the maximum temperatures and speeds reached during such interparticle collisions. Metal particles that were irradiated in hydrocarbon liquids with ultrasound underwent collisions at roughly half the speed of sound and generated localized effective temperatures between 2600°C and 3400°C at the point of impact for particles with an average diameter of ~10 μm.

THE CHEMICAL EFFECTS OF HIGH-intensity ultrasound result primarily from acoustic cavitation: the formation, growth, and implosive collapse of bubbles in liquids (*1–5*). In heterogeneous, solid-liquid reactions, ultrasound has increased the reactivity of metal powders by as much as 100,000-fold (*6*). Ultrasound has become an important tool in chemical synthesis involving mixed-phase reactions (*1–3, 7–9*). Studies on the effect of ultrasound on metal powders have shown dramatic changes in particle morphology, substantial agglomeration of powders, and significant reduction of passivating surface oxide coatings (*6, 10–15*). Still the origins of the dramatic enhancements observed with heterogeneous sonochemistry have remained unclear.

Acoustic cavitation in liquids generates implosive bubble collapse and associated shock waves. Bubble collapse near an extended surface can also produce localized, high-speed jets of liquid that impinge on the surface (*16–19*). Fine powders, however, are too small to perturb the ultrasonic field. At 20 kHz, for example, simple calculations indicate that the collapsing bubble will have a diameter of ~150 μm (*1, 19*); solid particles smaller than this size cannot cause microjet formation. In the presence of small particles, however, normal cavitational collapse will still occur.

The shock waves so generated can cause small particles to collide into one another with great force, producing interparticle melting, as illustrated in Fig. 1 for a Zn powder with an average diameter of 5 μm. The two Zn particles, originally separate spheres, are fused together after impact. The formation of a neck of Zn metal joining the two particles can be seen in the scanning electron micrograph. We believe that this neck originates from the rapid cooling of the effectively molten collision zone as the colliding particles rebound immediately after impact.

The Sn [<44 μm average diameter, mp (melting point) 232°C] and Fe (5 μm average diameter, mp 1535°C) particles were ultrasonically irradiated for 30 min in decane, which resulted in fusion of the different metal particles (Fig. 2). As in the case of the Zn particles, a melted neck joins the two particles. A scanning Auger electron spectroscopy dot map of elemental Sn shows that the Sn particle and the melted neck area to be made mainly of Sn, as expected from the relative melting points of the metals.

In order to determine roughly the maxi-

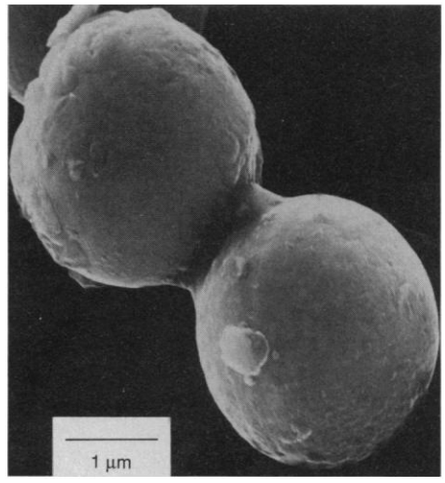

Fig. 1. Scanning electron micrograph of 5-μm average diameter Zn powder. Neck formation from localized melting is caused by high-velocity collisions. The metal powders (Mallinckrodt) were irradiated 30 min at 15°C in freshly distilled decane (17 ml, ~20% by weight) under Ar, with direct-immersion ultrasonic horn (Heat Systems) at 20 kHz and 50 W/cm^2. The slurry was then filtered, washed with pentane, and dried under vacuum at ~75°C for 24 hours. Scanning electron micrographs were taken on a Hitachi S-800 at 20-kV accelerating voltage.

School of Chemical Sciences, University of Illinois at Urbana-Champaign, Urbana, IL 61801.

*To whom correspondence should be addressed.

mum temperatures reached during interparticle collisions, a series of transition metal powders were irradiated as slurries in decane. Scanning electron micrographs were then obtained before and after irradiation (Fig. 3). Cr powder (mp 1857°C) before irradiation consisted of nonaggregated crystalline particles. After 30 min of irradiation, extensive interparticle fusion occurred, which resulted in the formation of large agglomerates. In addition, the original crystallinity of the individual particles had been reduced by irradiation, and the surface of the agglomerates showed considerable smoothing. Similar results also occurred with Ni powder (mp 1453°C) (*6*).

Molybdenum (mp 2617°C) also showed agglomeration and interparticle melting after 30 min of irradiation, but the effect of the interparticle collisions was noticeably lessened. The substantial neck formation, as seen in the Zn and Cr powders, was reduced in appearance to spot-welds. No change in surface morphology of the Mo particles could be observed, even with extended irradiation of 4 hours.

In contrast to Zn, Ni, Cr, and Mo powders, ultrasonic irradiation of W powder produced no appreciable effects (Fig. 3). No appreciable agglomeration and no changes in surface morphology of the W were noted, even with 4 hours of irradiation. Because W melts at 3410°C, we conclude that the peak effective temperatures reached during interparticle collisions must fall between roughly 2600°C and 3400°C for particles ~10 μm in diameter. The extreme, but short-lived, conditions created during these interparticle collisions will also have a high-pressure component; some plastic deformation below a true melting of the collision zone may also occur.

Interparticle velocities must depend on particle size; sufficiently large particles will be only minimally accelerated by the cavitation shock waves. Interparticle collisions still occur and surface morphology and chemical reactivity can be affected, but particle agglomeration will not occur; this is the case for 160-μm diameter Ni (*10*). Similarly, solvent viscosity is expected to influence the nature of interparticle collisions. In sufficiently viscous liquids, the velocity of interparticle collisions will probably be diminished. We have observed similar interparticle collisions in various synthetically useful liquids, including several alkanes (*n*-octane through *n*-tetradecane), dimethylformamide, and dioxane.

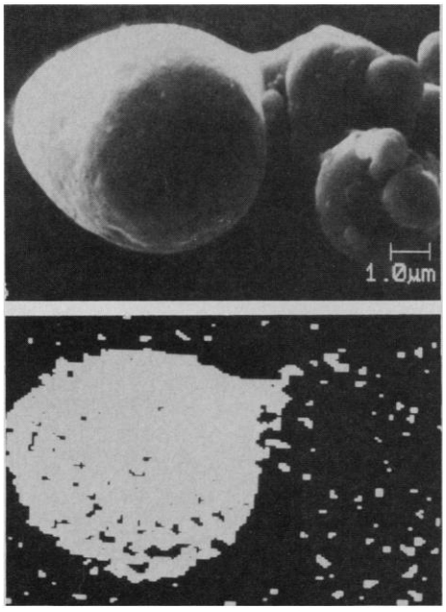

Fig. 2. (**Top**) Scanning electron micrograph of an interparticle collision induced by ultrasound between Sn (Alfa Products) and Fe (Cerac) particles. (**Bottom**) Elemental Sn dot map showing the Sn particle and melted neck region. Slurries treated as described in the legend to Fig. 1. Elemental composition determined by scanning Auger electron spectroscopy on a Perkin-Elmer 660 spectrometer at 20-kV and 0.46-nA current.

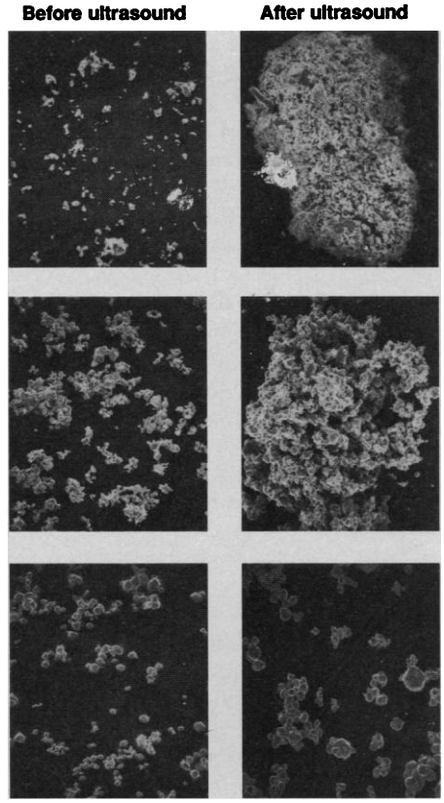

Fig. 3. The effect of ultrasonic irradiation on particle agglomeration of (**top**) Cr (3 μm average diameter, mp 1857°C; Alfa Products), (**middle**) Mo (10 μm average diameter, mp 2617°C; Aldrich), and (**bottom**) W (10 μm average diameter, mp 3410°C; Alfa Products) in decane slurries. The metal powders were irradiated for 30 min in decane slurries of 2.5% metal v/v, as described in the legend to Fig. 1. Size bar, 60 μm.

We can also estimate the velocity and time of interparticle impact from these studies. If we assume that full melting of the neck region of merged particles occurred during collision, then the energy of the collision can be calculated from heat capacities and heats of fusion applied to the volumes of the interparticle necks determined by scanning electron micrograph. The energies necessary to melt 1.0 μm^3 of Sn, Zn, Cr, and Fe are 0.012, 0.027, 0.12, and 0.13 ergs, respectively (*20*). Because the collisions have a range of interparticle velocities, there is an observed range of neck sizes in each experiment. Typically, the interparticle neck volumes are between 0.5 and 6 μm^3. The calculated energy to melt the neck represents a lower bound of the kinetic energy of impact and thus is a lower bound estimate of the impact velocity. Repeating this calculation for Zn-Zn, Cr-Cr, and Fe-Sn interparticle collisions from many micrographs results in estimates of impact velocities ranging from 100 m/s to 500 m/s, for particles ~10 μm in diameter.

For comparison, the speed of sound in hydrocarbons is roughly 1100 m/s. By definition, shock waves generated by cavitation will have velocities greater than the speed of sound. From thermodynamic models of underwater bomb blasts, one can estimate expected velocities for infinitesmal particles, based on the shock wave pressure (*21*). Measurements from laser-induced cavitation in water (*22*) yield shock wave pressures as large as 300 MPa, which would predict velocities of 160 m/s for infinitesimal particles, in agreement with our observations for 10-μm diameter powders.

Finally, we can estimate roughly the time of cooling of the melted neck formed during impact. If the colliding particles recoil with a velocity on the order of 500 m/s (an upper bound), then a neck with length of 0.5 μm would be formed in roughly a nanosecond. This is a reasonable lower limit estimate of the cooling time after collision of 10-μm diameter powders.

The dramatic effects of ultrasound on heterogeneous liquid-solid chemical reactions have already been well established. We have quantified the high-energy conditions created during ultrasonic irradiation of powders in liquids. These studies highlight the importance of high-velocity interparticle collisions during ultrasonic irradiation of metal slurries and illustrate the analogy between heterogeneous sonochemistry and tribochemistry or mechanochemistry. Particles that collide head-on do so with enough energy to cause localized melting at the site of impact. This reveals hot, reactive metal surfaces and contributes to the chemical effects of ultrasound.

REFERENCES AND NOTES

1. K. S. Suslick, Ed., *Ultrasound: Its Chemical, Physical, and Biological Effects* (VCH Publishers, New York, 1988).
2. K. S. Suslick, *Sci. Am.* **260**, 80 (February 1989).
3. ———, *Adv. Organomet. Chem.* **25**, 73 (1986).
4. ——— and E. B. Flint, *Nature* **330**, 553 (1987); E. B. Flint and K. S. Suslick, *J. Am. Chem. Soc.* **111**, 6987 (1989).
5. K. S. Suslick, R. E. Cline, Jr., D. A. Hammerton, *J. Am. Chem. Soc.* **108**, 5641 (1986).
6. K. S. Suslick and D. J. Casadonte, *ibid.* **109**, 3459 (1987).
7. K. S. Suslick, *Mod. Syn. Methods* **4**, 1 (1986).
8. C. Einhorn *et al.*, *Synthesis* **11**, 787 (1989).
9. J. Lindley and T. J. Mason, *Chem. Soc. Rev.* **16**, 275 (1987).
10. K. S. Suslick, D. J. Casadonte, S. J. Doktycz, *Solid State Ionics* **32/33**, 444 (1989).
11. ———, *Chem. Materials* **1**, 6 (1989).
12. K. S. Suslick and S. J. Doktycz, *Adv. Sonochem.*, in press.
13. ———, *J. Am. Chem. Soc.* **111**, 2342 (1989).
14. J. C. de Souza-Baroza, C. Petrier, J. L. Luche, *J. Org. Chem.* **53**, 1212 (1988).
15. J. Lindley, T. J. Mason, J. P. Lorimer, *Ultrasonics* **25**, 45 (1987).
16. W. Lauterborn and W. Hentschel, *ibid.* **24**, 59 (1985).
17. ———, *ibid.* **25**, 260 (1986).
18. C. M. Preece and I. L. Hansson, *Adv. Mech. Phys. Surf.* **1**, 199 (1981).
19. E. A. Neppiras, *Phys. Rep.* **61**, 159 (1980).
20. R. C. Weast, Ed., *CRC Handbook of Chemistry and Physics* (CRC Press, Boca Raton, FL, 1989), p. D-43.
21. R. H. Cole, *Underwater Explosions* (Princeton Univ. Press, Princeton, NJ, 1948).
22. A. Vogel and W. Lauterborn, *J. Acoust. Soc. Am.* **84**, 719 (1988).

24. We appreciate the use of the Center for Microanalysis of Materials, University of Illinois at Urbana-Champaign, supported by the U.S. Department of Energy under contract DE-AC-02-76ER-01198. Support of the NSF is greatly appreciated. K.S.S. gratefully acknowledges an NIH Research Career Development Award.

24 August 1989; accepted 13 December 1989

Gaussian Free-Energy Dependence of Electron-Transfer Rates in Iridium Complexes

LUCIUS S. FOX, MARIUSZ KOZIK, JAY R. WINKLER, HARRY B. GRAY

The kinetics of photoinduced electron-transfer (ET) reactions have been measured in a series of synthetic donor-acceptor complexes. The electron donors are singlet or triplet excited iridium(I) dimers (Ir_2), and the acceptors are *N*-alkylpyridinium groups covalently bound to phosphinite ligands on the Ir_2 core. Rate constants for excited-state ET range from 3.5×10^6 to 1.1×10^{11} per second, and thermal back ET (pyridinium radical to Ir_2^+) rates vary from 2.0×10^{10} to 6.7×10^7 per second. The variation of these rates with driving force is in remarkably good agreement with the Marcus theory prediction of a Gaussian free-energy dependence.

THE PRIMARY CHARGE SEPARATION in the bacterial photosynthetic reaction center proceeds in less than 5 ps and is virtually independent of temperature (*1*). Subsequent ET steps that increase the charge-separation distance, and ultimately lead to photochemical energy storage, are all faster than energy-wasting charge-recombination events (*2*). If we are to prepare synthetic systems that emulate natural photosynthesis, thorough comprehension of all factors governing ET rates is essential. In semiclassical ET theory, three parameters govern the reaction rates: (i) the electronic coupling between the donor and acceptor (κ_E), (ii) the free-energy change for the reaction ($\Delta G°$), and (iii) a parameter (λ) related to the extent of inner-shell and solvent nuclear reorganization accompanying the ET reaction (*3*). Moreover, when intrinsic ET barriers are small, the dynamics of nuclear motion can limit ET rates through the frequency factor ν_N. These parameters describe the rate of ET between a donor and acceptor held at a fixed distance and orientation (Eq. 1),

$$k_{ET} = \nu_N \kappa_E \exp\left[\frac{-(\Delta G° + \lambda)^2}{4\lambda RT}\right] \quad (1)$$

where R is the gas constant and T is the absolute temperature.

The surprising prediction of a Gaussian free-energy dependence for k_{ET} has stimulated numerous experimental investigations (*4–11*). Early attempts to verify Eq. 1 were frustrated by diffusion-limited rates at high driving forces in bimolecular ET reactions. Our previous examination of the ET quenching of the triplet excited state of $[Ir_2(\mu\text{-pz})_2(COD)_2]$ (pz = pyrazolyl; COD = 1,5-cyclooctadiene) by alkylpyridinium acceptors is a case in point (*6*). At driving forces between 0.1 and 0.8 eV, the quenching rate constant increases monotonically. At higher driving forces, the rates plateau at $10^{10} M^{-1}\ s^{-1}$. No evidence was found for a decrease in ET rate at driving forces up to 1.18 eV.

In order to circumvent the bimolecular diffusion limit, we have prepared a set of complexes in which the electron donor and acceptor are covalently coupled into one molecule, $[Ir_2(\mu\text{-pz}^*)_2(CO)_2(Ph_2PO(CH_2)_2A^+)_2]$ (pz* = 3,5-dimethylpyrazolyl; Ph = C_6H_5). The Ir(I) dimer (Ir_2) serves as the electron donor, and the acceptors (A^+) are *N*-alkylpyridinium groups bound to phosphinite ligands (Fig. 1). An x-ray crystal structure determination of the complex with A^+ = pyridinium (py^+) reveals a 5.8 Å separation between the closer Ir center and the N atom of the pyridinium ring (*12*). In its lowest singlet (^1B) and triplet (^3B) excited states, the Ir_2 chromophore is a potent reductant that is capable of transferring an electron to a covalently attached pyridinium cation (*12, 13*).

We reported previously that ET quenching of the ^1B excited state in two of the donor-acceptor complexes (A^+ = pyridin-

Table 1. Photophysical parameters for Ir_2-phosphinite complexes (Me, methyl; Et, ethyl). Quantum yields (ϕ_f, singlet quantum yield; ϕ_p, triplet quantum yield) taken from spectra measured in acetonitrile solutions at room temperature with Ru(2,2′-bipyridine)$_3^{2+}$ used as a standard; excitation wavelength = 436 nm (*25*). Singlet quantum yields for the reference complexes are ±10%; triplet quantum yields are ±30%. Singlet quantum yields for the donor-acceptor complexes are ±30%; triplet quantum yields are ±80%. Singlet lifetime is τ_f; triplet lifetime is τ_p.

Phosphinite	ϕ_f	ϕ_p	τ_f (ps)	τ_p† (μs)
	Reference complexes			
$Ph_2POCH_2CH_2\text{-}NEt_3^+$	0.0015	0.032	95*	1.2
$Ph_2POCH_2CH_3$	0.0023	0.025	100*	1.1
Ph_2POCH_3	0.0027	0.040	100‡	1.2
$Ph_2PO(CH_2)_3CH_3$	0.0025	0.030	100‡	1.1
	Donor-acceptor complexes			
$Ph_2POCH_2CH_2Me_3py^+$	0.00017	0.0013	25†	0.012 0.144
$Ph_2POCH_2CH_2\text{-}4\text{-}Mepy^+$	0.00006	0.0004	9†	0.003
$Ph_2POCH_2CH_2\text{-}py^+$	0.00003	§	4.4‖	§

*Determined from transient absorption measurements; ±20%. †Determined from time-resolved emission measurements; ±10%. ‡Estimated from quantum yields and the singlet lifetime of $[Ir_2(pz^*)_2(CO)_2(Ph_2POCH_2CH_3)_2]$; ±10%. §Emission too weak to measure. ‖Estimated from quantum yields and singlet lifetime of $[Ir_2(pz^*)_2(CO)_2(Ph_2POCH_2CH_3)_2]$; ±30%.

L. S. Fox and H. B. Gray, Arthur Amos Noyes Laboratory, California Institute of Technology, Pasadena, CA 91125.
M. Kozik and J. R. Winkler, Department of Chemistry, Brookhaven National Laboratory, Upton, NY 11973.